Yuhang Chen
School of Aerospace,
Mechanical and Mechatronic Engineering,
The University of Sydney,
Sydney, NSW 2006, Australia

Michiel Schellekens
Department of Mechanical Engineering,
Eindhoven University of Technology,
P.O. Box 513, 5600 MB Eindhoven,
The Netherlands

Shiwei Zhou

Joseph Cadman

Wei Li

School of Aerospace,
Mechanical and Mechatronic Engineering,
The University of Sydney,
Sydney, NSW 2006, Australia

Richard Appleyard
School of Medicine,
Macquarie University,
NSW 2109, Australia

Qing Li[1]
Member of ASME,
School of Aerospace,
Mechanical and Mechatronic Engineering,
The University of Sydney,
Sydney, NSW 2006, Australia
e-mail: Qing.Li@Sydney.edu.au

Design Optimization of Scaffold Microstructures Using Wall Shear Stress Criterion Towards Regulated Flow-Induced Erosion

Tissue scaffolds aim to provide a cell-friendly biomechanical environment for facilitating cell growth. Existing studies have shown significant demands for generating a certain level of wall shear stress (WSS) on scaffold microstructural surfaces for promoting cellular response and attachment efficacy. Recently, its role in shear-induced erosion of polymer scaffold has also drawn increasing attention. This paper proposes a bi-directional evolutionary structural optimization (BESO) approach for design of scaffold microstructure in terms of the WSS uniformity criterion, by downgrading highly-stressed solid elements into fluidic elements and/or upgrading lowly-stressed fluidic elements into solid elements. In addition to this, a computational model is presented to simulate shear-induced erosion process. The effective stiffness and permeability of initial and optimized scaffold microstructures are characterized by the finite element based homogenization technique to quantify the variations of mechanical properties of scaffold during erosion. The illustrative examples show that a uniform WSS is achieved within the optimized scaffold microstructures, and their architectural and biomechanical features are maintained for a longer lifetime during shear-induced erosion process. This study provides a mathematical means to the design optimization of cellular biomaterials in terms of the WSS criterion towards controllable shear-induced erosion. [DOI: 10.1115/1.4004918]

Keywords: wall shear stress, topology optimization, scaffold, biofluid, biodegradation

1 Introduction

As a fundamental premise of tissue engineering, scaffold is expected to provide a replicable biomechanical environment for the damaged tissues or organ and a proper level of permeability for cell diffusion, nutrient delivery and metabolite removal [1]. Firstly, a physiological range of wall shear stress (WSS) at the microstructural surfaces of scaffold is favorable for promoting cellular attachment and mechanobiological response [2,3]. Secondly, WSS plays a vital role in the shear-induced erosion of biodegradable polymer, which raises a key issue of how to regulate WSS towards a controllable erosion process [4,5]. For this reason, the design optimization of scaffold micro-architecture signifies an important topic of research in seeking a desirable distribution of resultant WSS, especially for achieving a better cellular mechanobiological response and polymeric erosion outcome in tissue-scaffold systems [6].

The bio-fluidic phase of tissue-scaffold system offers a critical function for mass transport, in which WSS is one of the key factors that make impact on tissue regeneration. Firstly, there have been a range of studies available to date in understanding the mechanobiological function of WSS in bone tissue engineering [7]. As a matter of fact, WSS plays a regulatory role in osteoblastic response to external mechanical stimulus [8], in which a certain level of WSS was confirmed to increase the mRNA expression [9] and promote tissue growth [10], thus improving the tissue regeneration outcome. Recently, Kwon and Jacobs [2] performed an *in vitro* test on time-dependent deformation of bone cells subject to fluid flow, which was found to be a primary physical stimulus in regulating the bone cell metabolism. Adachi et al. [11] proposed a theoretical model for trabecular bone remodeling, in which the role of fluid-induced shear stress in osteocytic mechanosensory network system was verified. Secondly, WSS is also critical to the cellular attachment on scaffold surfaces. It has been observed that, for endothelial cells, cellular detachment would occur when the fluidic shear exceeded a certain threshold [3], which implies that a relatively lower level of flow shear stress would be beneficial for facilitating cell attachment onto the scaffold wall surfaces [12]. Taken into account these two important issues mentioned above, an optimal level of WSS required by the cellular 'mechanosensory' and 'attachment' criteria might be somewhat contradictory. Therefore, a uniform distribution of WSS at the physiological level that allows promoting cellular response and attachment would be beneficial in general.

Apart from the biological roles of WSS, its physical and chemical concerns have also attracted increasing attention,

[1]Corresponding author.

Contributed by the Bioengineering Division of ASME for publication in the JOURNAL OF BIOMECHANICAL ENGINEERING. Manuscript received April 19, 2011; final manuscript received August 18, 2011; published online September 19, 2011. Assoc. Editor: Stephen Klisch.

particularly in the fluid-driven mechanical erosion of polymers. It has been concluded that the shear stress represents a key factor to induce polymeric chain scission [13], where the degradable polymers were found to have an approximate midpoint chain scission in dilute solution under fluid flow [14]. Furthermore, both experimental [5] and mathematical [4] approaches were conducted to explore the erosion and breakup of polymer particles under shear flow, which was considered a key factor for erosion mechanism. More recently, it was validated that WSS induced by fluid flow provides mechanical energy that leads to the chain scission and lessens the drag reduction effectiveness [15]. Therefore, the function of WSS that determines the surface erosion of polymers should be addressed when designing polymeric tissue scaffolds, particularly under high-shear conditions, e.g., within bioreactors [16]. To date, there have been some reports available concerning modeling such a flow-induced erosion process, in which the rate of mechanical degradation was related to the surface shear stress [5,17]. For this reason, it is beneficial to regulate WSS to a desirable or even uniform level so that the flow-induced erosion can be controlled or even minimized (when required) for specific purposes, e.g., maintaining the stiffness and strength of scaffold to a level above a certain threshold as long as possible [18].

In the recent years, use of periodic scaffold microstructure has become rather prevalent due to its more controllable effective properties and advantageous features of design optimization [19]. Latest development of solid free-form fabrication (SFF) has made this approach even more attractive by providing an effective means to the fabrication of highly sophisticated periodic microstructures [20–23]. Note that, of various design methods, topology optimization has been one of the most successful approaches that allow the design of periodic microstructures with desirable effective mechanical properties, ranging from stiffness [24], conductivity [25,26] to some other multidisciplinary criteria [27–29]. Recently, significant effort has been devoted to various fluidic criteria, e.g., desirable or maximized permeability [30] or diffusivity [31]. However, there have been very limited studies available on the WSS-based design and its implication in shear flow-induced erosion of biodegradable polymers has remained unclear.

This paper proposes a bi-directional evolutionary structural optimization (BESO) procedure for bio-fluid problems, in which the uniformity of WSS is adopted as the design criterion to seek the optimal scaffold architecture. As an elegant heuristic approach, BESO has proven fairly simple and effective in coping with both gradient and nongradient topology optimization problems [32,33]. In this paper, we will show how this approach can be extended to a new sphere of fluidic optimization with considerable sophistications in design conditions and topological variation.

Following the WSS-based topology optimization, a shear-induced erosion model is developed to evaluate the erosion rate and patterns for the baseline and optimal scaffolds. The homogenization method is also implemented to obtain the effective stiffness and permeability throughout the erosion process for the baseline and optimal designs. The illustrative examples with various initial designs under different flow conditions are presented to demonstrate the effectiveness of proposed design and characterization approaches.

2 Materials and Methods

2.1 Bio-Fluid Characterization. Bio-fluid within scaffold microstructures transports nutrients and metabolites for osteocytes and forms a crucial component to maintain newly-regenerated tissue alive. More importantly, it can induce various forms of mechanical stimuli on osteocytes via solid-fluid interaction to uphold the mechanosensory and remodeling activities in bony tissue [34]. In this regard, understanding and characterization of bio-fluid within bone/scaffold are of great importance.

Bio-fluid in bone mainly comprises serum and extracellular flow, which can be characterized by the Darcy's law of diffusion in porous medium [35]. Similarly, the in-scaffold bio-fluid *in vivo* or under static condition *in vitro* can also be considered as such a flow condition with a relatively low Reynolds number. However, for the scaffold subject to a preculturing condition within a bioreactor, flow status sometimes become much more complex due to sophisticated scaffold micro-architectures and operational conditions of bioreactor systems [36]. Nevertheless, to model the bio-fluid for topology optimization and shear-induced erosion, the flow within scaffold micro-architecture is often considered Newtonian and incompressible [37], in which the steady-state Navier-Stokes equation can be used as

$$\rho(\mathbf{u}\cdot\nabla\mathbf{u}) = -\nabla p + \mu\nabla^2\mathbf{u} \tag{1}$$

where ρ denotes the density of fluid, $\mathbf{u}$ the fluid velocity, p the pressure and μ the dynamic viscosity. On the wall surface of solids, a nonslip boundary condition can be applied. Thus the wall shear stress can be directly calculated in terms of flow velocities, u, v and w, under Cartesian coordinate system as

$$\tau_w = \sqrt{\left[\mu\left(\frac{\partial u}{\partial y}+\frac{\partial v}{\partial x}\right)\right]^2+\left[\mu\left(\frac{\partial v}{\partial z}+\frac{\partial w}{\partial y}\right)\right]^2+\left[\mu\left(\frac{\partial u}{\partial z}+\frac{\partial w}{\partial x}\right)\right]^2} \tag{2}$$

2.2 BESO Method. As mentioned above, it is desirable to generate a certain level of WSS within the scaffold microstructure for controlling both mechanobiological tissue regeneration and shear-induced erosion. For this purpose, topology optimization is applied here to seek optimal 3D RVE structure that provides uniform WSS, which can be mathematically formulated as

$$\begin{cases} \min \quad F = \displaystyle\int_\Gamma (\tau_w-\bar{\tau}_w)^2 d\Gamma \cong \sum_{e=1}^{NIE} w_\Gamma^e(\tau_w^e-\bar{\tau}_w)^2 \\ s.t. \quad V_s = \displaystyle\int_{\Omega_s} \rho^e d\Omega_s = V_c \end{cases} \tag{3}$$

where $\Gamma = \partial\Omega_s \cup \partial\Omega_f$ denotes the solid-fluid interface, *NIE* is the number of interfacial elements and w_Γ^e the interfacial area of element e. Note that the design domain consists of fluid and solid phases ($\Omega = \Omega_f + \Omega_s$), and ρ^e represents the relative density of elements, specifically $\rho^e = 0$ for fluid phase Ω_f and $\rho^e = 1$ for solid phase Ω_s in the topology optimization procedure. The overall objective function F is defined as the least square of elemental shear stress τ_w^e and target (e.g., mean) shear stress $\bar{\tau}_w$, subject to a volume constraint V_c of solid phase V_s (where V_s denotes the volume fraction of solid phase in the topology optimization) in the design domain.

Since the wall shear stress calculated from Eq. (2) is typically a nodal quantity, it is necessary to convert the nodal WSS into an elemental variable for the element-based BESO approach. For a regular 3D brick element, this can be calculated in terms of average value as

$$\tau_w^e = \frac{1}{ND}\sum_{i=1}^{ND}\tau_w^i \tag{4}$$

where τ_w^e denotes elemental WSS, τ_w^i the nodal solution and *ND* the number of nodes in the element considered. Once the elemental WSS is obtained, relative ranking can be made for the interfacial solid ($e\in\partial\Omega_s$) and interfacial fluid ($e\in\partial\Omega_f$) elements, respectively. Then two different algorithms are implemented herein to attain an optimal objective defined in Eq. (3), i.e., to minimize the difference between local (elemental) and target WSS. One is to downgrade the highly stressed interfacial solid elements into fluidic elements at the interface (i.e., $\rho^e = 1 \rightarrow \rho^e = 0$); and the other is to upgrade the lowly stressed fluidic interfacial elements into solid

elements (i.e. $\rho^e=0 \rightarrow \rho^e=1$). For each iteration, if the volume fraction of solid phase exceeds the prescribed constraint ($V_s > V_c$), the solid elements ($\rho^e=1$) with highest WSS would be changed into the fluidic elements ($\rho^e=0$); on the other hand, if the current volume fraction is lower than the constraint ($V_s \leq V_c$), the fluidic elements ($\rho^e=0$) with lowest WSS would be changed into the solid elements ($\rho^e=1$). To ensure the scaffold volume converging towards a predefined constraint, the volume variation ratio υ is gradually reduced in terms of a small rate constant $R^{(k)}$, as

$$\Delta V^{(k)} = (R^{(k)}\upsilon)V \tag{5}$$

where V denotes the total volume of fluid and solid phases in the design domain and $\Delta V^{(k)}$ is the volume of elements subject to the change between solid and fluid elements at the kth iteration. In the following examples, $R^{(k)}=0.01$ and volume variation ratio $\upsilon=0.97$ are adopted. As the optimization progresses, the volume change in the BESO algorithm gradually decreases in each iteration. As such, a more uniform distribution of WSS is achieved in the solid-fluid interface; at the same time the prescribed constraint of volume fraction can be attained.

There are some numerical issues to be addressed herein. Firstly, the number of solid elements that are removed (downgraded) or added (upgraded) in the early stage can be relatively greater than that in a traditional BESO procedure [38]. Thus the design can quickly evolve from initial topology towards the optimum. Secondly, newly-formed solid elements are allowed to present only when a solid element exists at the adjacent places, thereby avoiding the 'checkerboard' pattern or isolated islands [39]. Finally, symmetry conditions are applied in the examples below wherever possible.

With regard to the convergence of BESO procedure, the standard deviation of objective values over the last five consecutive iterations is used [33]. The optimization is considered convergent when it is within a certain convergence tolerance ε, mathematically expressed as

$$\sqrt{\frac{1}{5}\sum_{k=1}^{5}[F^{(k)}-\bar{F}]^2} \leq \varepsilon \tag{6}$$

where $F^{(k)}$ is the kth objective value and $\bar{F}$ is the average of last five consecutive objectives.

2.3 Shear-Induced Polymer Erosion. In the topology optimization scheme, as given by Eq. (3), the elemental density is used as the design variable. Meanwhile, elemental density can represent the normalized dimensionless average molecular weight provided that the number of elements is sufficiently high, as suggested in the previous study of modeling polymer degradation [40]. In other words, elemental density ρ^e (1 or 0) in the BESO approach also represents the local polymer status in order to model the shear-induced polymeric erosion, i.e., 1 representing the *noneroded* status while 0 the *eroded* status. Following the erosion mechanism proposed by Culter et al. [41], a WSS threshold $[\tau_{ero}]$ is adopted to determine whether or not the chain scission would take place, i.e.,

$$\rho^e = \begin{cases} 1; & \tau_w^e < [\tau_{ero}] \\ 0; & \tau_w^e \geq [\tau_{ero}] \end{cases} \tag{7}$$

If the elemental WSS on the solid wall surface exceeds the threshold, the polymer chain in this element is assumed to be fully dissolved in the specific time step and then it will be washed away from solid boundary into a fluid element. If elemental WSS is below the erosive threshold, this element remains unaffected in the structure at the current time step. This process continues until all the solid elements are eroded or the WSS of all remaining elements are below the erosive threshold, leading to a stabilized status of shear-induced erosion process. It must be pointed out that there is no specific time scale involved in the proposed erosion model and we use the term 'time step' to denote the iteration process. Throughout the entire process, the WSS threshold $[\tau_{ero}]$ is predefined and remains unchanged, which allows yielding comparable erosion outcomes between initial and optimized scaffolds under the same conditions. Nevertheless, any experimental data of WSS threshold from fluid-induced erosion tests can be implemented into the algorithm to generate a time-specific simulation once available.

2.4 Scaffold Periodicity and Homogenization Method. In this study, we would like to focus on a specific category of scaffolds, i.e., those with cellular (periodic) microstructures, which has drawn significant attention due to its designable architectures and programmable effective properties via the solid free-form fabrication (SFF) technique [20]. To characterize the periodicity of scaffold, the design domain is extracted from scaffold periodic microstructure as a base cell or representative volume element (RVE), where the periodic conditions are applied and given as

$$\begin{aligned} &\rho_m(\tilde{\mathbf{x}}) = \rho_M(\mathbf{x},\delta) \\ &\langle\tilde{\mathbf{x}}\rangle \ll \langle\mathbf{x}\rangle \end{aligned} \tag{8}$$

where ρ_m and ρ_M are two different expressions of elemental density under microscopic coordinates $\tilde{\mathbf{x}}$ and macroscopic coordinates $\mathbf{x}$. δ represents the periodicity index and $\langle\cdot\rangle$ denotes the span modulus in micro- or macro-scales [42].

Since it has been well-known that the microstructure of porous or multiphasic materials plays a decisive role in effective (bulk or macroscopic) properties [43], it is thus crucial to quantitatively define the relationship between these two distinct length scales. Following the mathematical derivations of the homogenization method (interested readers may wish to refer to the article by Hassani and Hinton [42] for a detailed review of the homogenization procedure), the energy form of effective stiffness tensor $\mathbf{C}^{\mathbf{H}}$ can be given as

$$\mathbf{C}^{\mathbf{H}}_{pqrs}\varepsilon^{0(kl)}_{pq}\varepsilon^{0(ij)}_{rs} = \frac{1}{|\mathbf{Y}|}\int_Y \left[(\varepsilon^{0(kl)}_{pq} - \varepsilon^{*}_{pq}(\mathbf{u}^{kl})\right]^T \mathbf{C}_{pqrs}\left[\varepsilon^{0(ij)}_{rs} - \varepsilon^{*}_{rs}(\mathbf{u}^{ij})\right] dY \tag{9}$$

where $\mathbf{C}$ is the stiffness tensor of a solid base material and $\mathbf{Y}$ the periodicity. ε^0 denotes the test strain field and ε^* the fluctuation strain field induced by the inhomogeneity of RVE. The characteristic displacement field $\mathbf{u}^{kl}$ can be obtained by solving

$$\int_Y C_{ijpq}\frac{\partial u_p^{kl}}{\partial y_q}\frac{\partial v_i}{\partial y_j}dY = \int_Y C_{ijpq}\varepsilon^{0(kl)}_{pq}\frac{\partial v_i}{\partial y_j}dY \tag{10}$$

where ε^0 is chosen as the unit vectors for simplicity [43]

By introducing the finite element method (FEM) into the homogenization equations, the effective stiffness tensor can be rewritten by substituting unit test strains ε^0 into Eq. (9), as

$$\mathbf{C}^{\mathbf{H}}_{ijkl} = \frac{1}{|\mathbf{Y}|}\sum_e |\mathbf{Y}^e|[(\mathbf{u}^e_0(\varepsilon^0_{ij}) - \mathbf{u}^e(\varepsilon^*_{ij})]^T \mathbf{K}^e_{ijkl}(\rho^e)[\mathbf{u}^e_0(\varepsilon^0_{kl}) - \mathbf{u}^e(\varepsilon^*_{kl})] \tag{11}$$

where $\mathbf{K}^e(\rho^e)$ is the local stiffness matrix of element e as a function of elemental density ρ^e. $\mathbf{u}^e_0(\varepsilon^0_{ij})$ and $\mathbf{u}^e(\varepsilon^*_{ij})$ are the nodal displacements associated with the unit test strain ε^0_{ij} and fluctuation strain field ε^*_{ij}, respectively. Thus, if the structure (often characterized by the density distribution function) of RVE and the periodicity $\mathbf{Y}$ are given, it is convenient to obtain the effective stiffness tensor $\mathbf{C}^{\mathbf{H}}$ through Eq. (11).

Similarly, the effective permeability of scaffold microstructure can be defined as [28]

$$P_{ij}^{\mathbf{H}} = \frac{1}{|Y|}\sum_{e}\mathbf{p}_{ij}^{e}(\rho^{e})\left(1-\frac{\partial\chi_i}{\partial y_j}\right) \tag{12}$$

where $\mathbf{p}^e(\rho^e)$ is the local permeability tensor as a function of elemental density ρ^e. χ_i is a solution to the characteristic equation

$$\frac{\partial}{\partial y_i}\left[\mathbf{p}_{ij}(y)-\mathbf{p}_{ij}(y)\frac{\partial\chi(y)}{\partial y_j}\right]=0 \tag{13}$$

Based on the homogenization procedure, the effective stiffness and permeability of scaffold microstructure can be obtained; therefore the evolution of mechanical properties can be modeled during erosion process.

2.5 Numerical Implementation. In the recent years, computational fluid dynamics (CFD) has been found particularly promising for predicting the fluid behavior within scaffold microstructures. Existing studies explored the flow conditions in a number of tissue engineering scenarios, such as cylindrical scaffolds [44], shear stress in 3D scaffolds with different pore geometries [45], and WSS and other mechanical stimuli in porous scaffold structures in bioreactors [46,47], which offered vital biomechanical insights into the characterization of bio-fluidic environment within porous scaffolds, thereby overcoming the difficulties of various experimental means and shortening the traditional trail-and-error process. Following such existing work, the design domain is discretized into $60\times60\times60$ elements in all the following examples. The density and dynamic viscosity of fluidic phase are both considered constant with the values of 1000 kg/m^3 and 8.2×10^{-4} kg m^{-1} s^{-1}, respectively [45].

In the BESO algorithm, each element in the RVE domain has only two status, either void (bio-fluid; $\rho=0$) or solid (material; $\rho=1$). Thus, for the homogenization approach, the elemental isotropic stiffness and permeability tensors of bio-fluid and scaffold matrix are also linked to the elemental status (density) in terms of Young's modulus E and permeability coefficient p, respectively. To be more specific, the Young's modulus and Poisson's ratio of polylactide (PLA) materials are adopted here as 1 GPa and 0.35, while the permeability coefficient of void phase is set as 1×10^{-14} m^4/N/s

$$E=\begin{cases}1\ GPa; & \rho=1\ (\text{solid/material})\\ 1\times10^{-5}\ GPa; & \rho=0\ (\text{void/bio-fluid})\end{cases} \tag{14}$$

$$p=\begin{cases}1\times10^{-19}\text{m}^4/\text{N/s}; & \rho=1\ (\text{solid/material})\\ 1\times10^{-14}\text{m}^4/\text{N/s}; & \rho=0\ (\text{void/bio-fluid})\end{cases} \tag{15}$$

To simulate the fluid characteristics in a periodic scaffold microstructure, it is assumed that the flow in structural (macroscopic) scale undergoes the same level of pressure loss throughout each RVE in macroscopic scale. Thus the periodic boundary conditions can be approximated by a pair of velocity and pressure boundaries on the opposite faces with prescribed pressure difference [46]. Without loss of generality, the inlet velocity is set as 50 μm s^{-1} and zero-pressure condition is applied on the opposite surface, indicating a constant pressure drop through each RVE.

A flow chart is provided in Fig. 1 to clarify the whole procedure of BESO topology optimization and shear-induced erosion algorithms, which specifically describes:

- Topology optimization of scaffold micro-architecture (Do iteration):
  (1) Determine the initial guess and proper boundary conditions for CFD analysis
  (2) Calculate elemental WSS and its relative ranking for interfacial solid and fluidic elements
  (3) Apply the BESO procedure: downgrade solid elements and/or upgrade fluidic elements towards a more uniform WSS until convergence

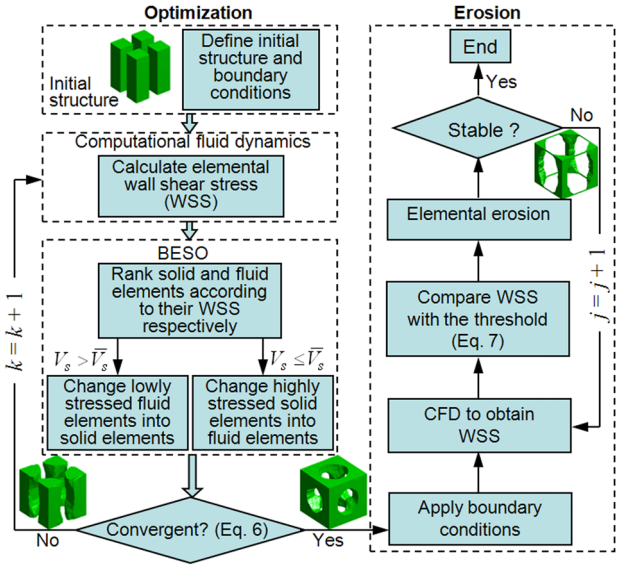

Fig. 1 Flow chart of BESO topology optimization and shear-induced erosion algorithms

- Shear-induced erosion simulation for scaffold microstructure (For time step):
  (1) Calculate the elemental WSS in the scaffold microstructure
  (2) Compare the WSS magnitude against the prescribed erosive threshold [τ_{ero}] to determine the elemental erosive status

3 Results

To demonstrate the effectiveness of the proposed methods, several examples with different flow conditions and initial designs are presented below.

3.1 90 deg Turn Pipe – A Benchmark Test. To validate the proposed BESO topology optimization method, a benchmark problem of a 90 deg turn pipe is firstly presented here [48–50]. An initial design with only 5% solid material is considered, which is allocated in the 12 edges (i.e., a truss structure) of the cubic design domain. The volume constraint V_c of solid phase is set as 90%, where a volume difference of 85% between initial design and prescribed constraint is deliberately presented in order to validate the proposed BESO approach. A circular inlet (A) is placed on the bottom surface, while a circular outlet (B) is connected to the lateral surface as shown in Fig. 2(*a*). Figure 2(*b*) illustrates the optimized fluid domain in terms of the WSS criterion, in which the design domain converges to a single bent pipe. The optimized configuration shows good agreement with the benchmark solution in literature [48,49]. Figure 2(*c*) plots the evolutionary history of objective function and volume fraction. It can be seen that the volume fraction of solid phase gradually converges to its constraint from 5% to 90% over these 120 iterations. In addition, the WSS spectrum in Fig. 2(*d*) exhibits a relatively narrow band of distribution, confirming that wall shear stress within the optimized structure becomes more uniform after the optimization.

3.2 Designs Under Tri-Directional Flow. In the second example, the initial design is defined as four isolated bars in the vertical direction. To generate a tri-directional flow within RVE, the prescribed pressure conditions are applied on all three pairs of corresponding faces. Figure 3(*a*) shows the evolutionary history and snapshots of topological changes during the optimization. It is observed that, the solid material is shifted from the highly-stressed region to the lowly-stressed region. As such, the initial design of four columns gradually evolves into a typical Schwarz-P structure [51].

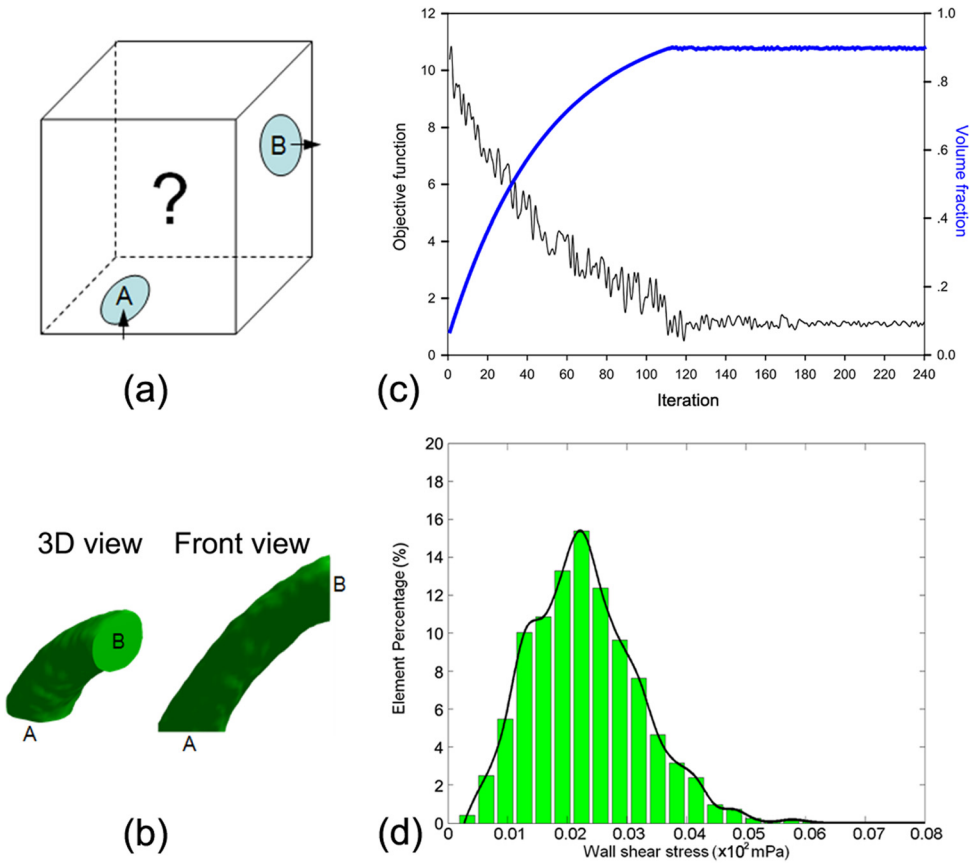

Fig. 2 Benchmark design example of a 90 deg turn pipe. (*a*) Design problem; (*b*) Optimal fluid structure; (*c*) Evolutionary histories of objective function and volume fraction of solid phase; and (*d*) WSS histogram after the optimization.

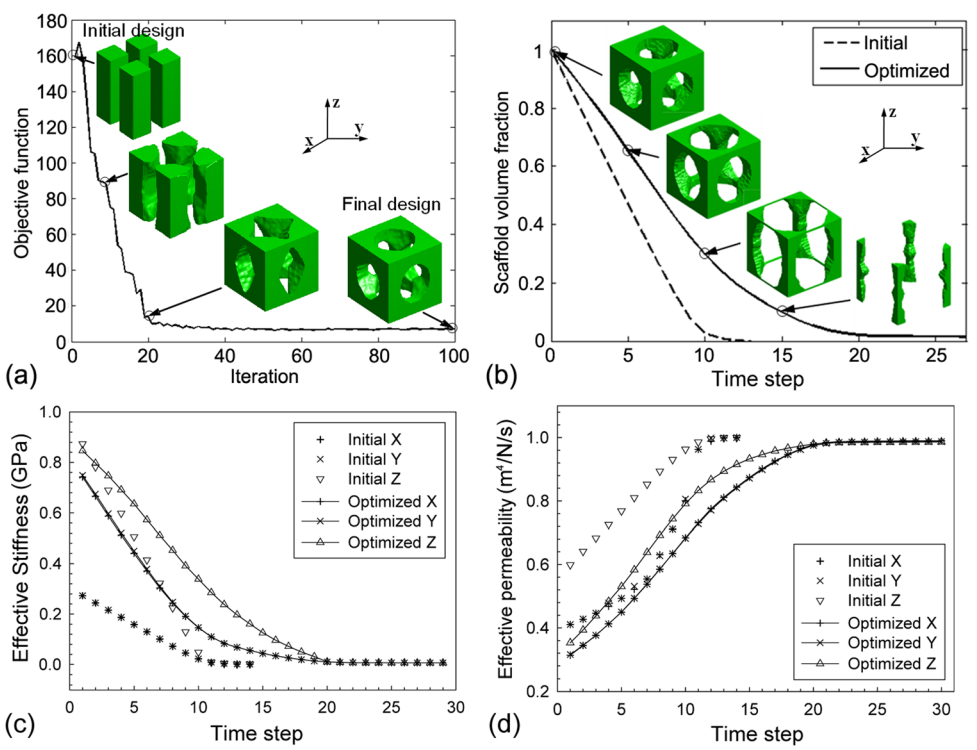

Fig. 3 Design optimization of scaffold micro-architecture under tri-directional flow with the initial design of four isolated vertical bars. (*a*) Convergence history and topological snapshots during optimization; and (*b*) Shear-induced erosion histories of initial and optimized designs; (*c*)–(*d*) Effective stiffness and permeability components of the initial and optimized scaffold designs.

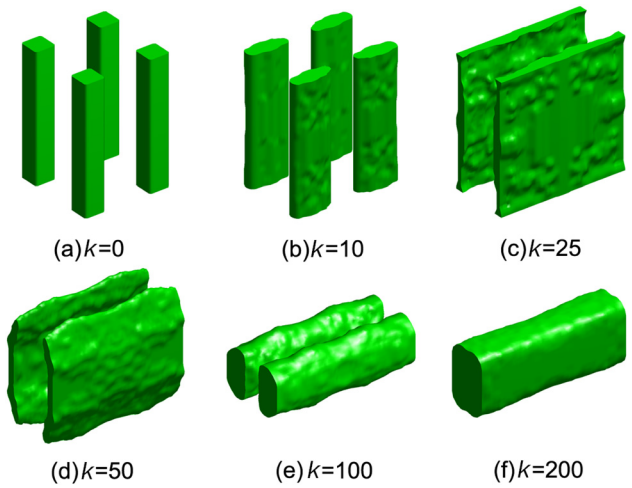

Fig. 4 Topological evolutions during design optimization under mono-directional flow (*k* denotes the iteration number). Initial design: four isolated vertical bars.

After the optimization, the erosion processes of both initial design (four vertical columns) and optimized architecture (Schwarz-P) are examined. Note that all the elements will be eroded if the threshold is too high while no elements are eroded if it is too low, the threshold is chosen such that degradation is allowed to take place in a progressive way but will remain unchanged for each problem, making the comparison of erosive processes between the initial and optimal designs possible. The results are plotted in Fig. 3(*b*), where the change in scaffold volume and relevant structural snapshots during shear-induced erosion are displayed. It is clear that the optimal design exhibits a significantly slower erosion rate than the initial design all the way through the entire shear-induced erosion process and takes a considerably longer lifetime to be fully dissolved.

The variations of effective stiffness and permeability components of both initial and optimized scaffold designs predicted by the homogenization method are shown in Figs. 3(*c*) and 3(*d*), respectively. For the effective stiffness, it can be found that all the stiffness components in both designs decrease dramatically as the erosion progresses, while the stiffness of the optimized scaffold can last more than 17 time steps compared to the initial design which lasts much fewer time steps. On the other hand, the flow-induced erosion significantly enhances the effective permeability in both cases. Increase of the effective permeability is slower in the optimal design than that in the initial design, indicating an opposite trend to the variation of the effective stiffness. Nevertheless, it should be noted that the optimized design maintains its main architectural features over almost 20 time steps while the microstructure of initial design quickly disappeared under flow-induced erosion within 10 time steps, losing almost all stiffness and strength.

3.3 Designs Under Mono-Directional Flow. The third example adopts the same initial design as the second one, but using a smaller constraint of volume fraction ($V_c = 0.1$). Only one pair of prescribed velocity-pressure conditions is applied to generate a mono-directional flow, while periodic conditions are applied on the other pairs of lateral surfaces to mimic the scaffold microstructure. Figure 4 illustrates the initial, intermediate and final designs, respectively. It is observed that these four columns stretch along the flow direction in the first 10 iterations, and gradually form two thin plates parallel to the flow direction ($k = 25$). Interestingly, these two thin plates further form two thick bars ($k = 100$), which finally merge into a single and thicker bar ($k = 200$).

Figure 5(*a*) compares the WSS distributions in the initial and optimal designs. It can be seen that the WSS spectrum changes from a spread-out distribution into a very sharp peak that indicates a much more uniform WSS. Following the optimization, the erosion process is simulated as illustrated in Fig. 5(*b*). Similarly to example 2, the optimized design exhibits a much longer erosion lifetime than the initial one.

To investigate whether the solution is dependent on the initial guess, we attempted another trusslike structure subjected to a horizontal flow. The topological evolutions are illustrated in Fig. 6(*a*). It is seen that the through-holes on the lateral surfaces gradually shrink, while the channel in the flow direction grows progressively, resulting in a single through channel for such a mono-directional flow. Figure 6(*b*) exhibits the WSS spectrums of initial and optimal designs.

The erosion simulations of initial and optimized designs are shown in Fig. 7. It is found in Fig. 7(*a*) that, although the initial design has a slightly slower erosion rate in the first 18 time steps, the optimal design erodes much more slowly in the later stage. Moreover, since the lateral surfaces of optimized structure are disconnected under mono-directional shear flow, only effective stiffness and permeability components in the x direction are presented in Figs. 7(*b*) and 7(*c*), in which they present similar trends to the results shown in Fig. 3(*c*)–3(*d*).

4 Discussion

This paper proposes a bi-directional evolutionary structural optimization (BESO) approach to seeking the optimal scaffold microstructures in different circumstances, in which an elemental manipulation algorithm is implemented for the WSS uniformity criterion, i.e., the solid elements with a higher level of WSS are

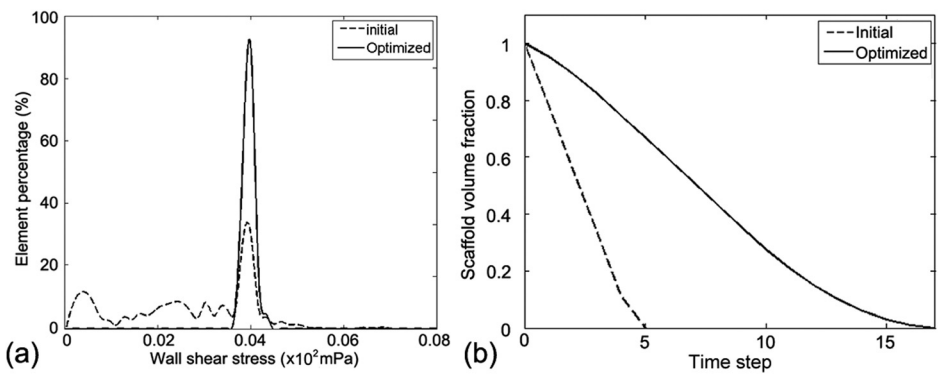

Fig. 5 Design optimization under mono-directional flow. Initial design: four isolated vertical bars. (*a*) Wall shear stress histogram and (*b*) erosion processes of the initial and optimal structures.

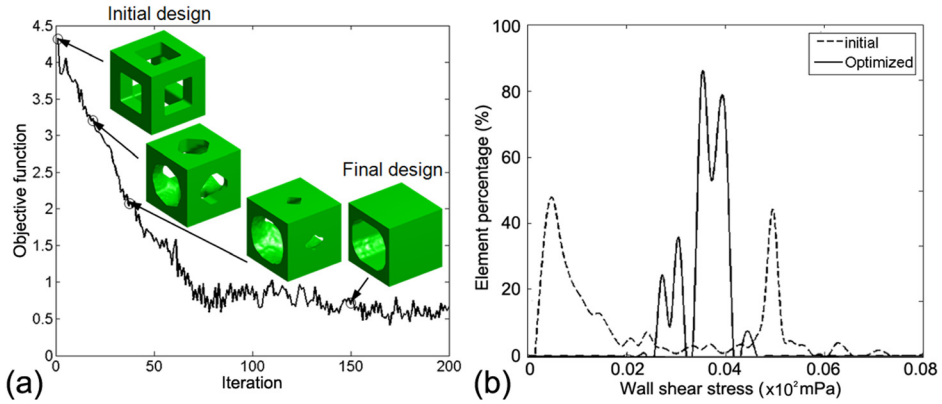

Fig. 6 Design optimization of scaffold micro-architecture under mono-directional flow. Initial design: inter-connected bars. (*a*) Convergence history and topological snapshots during optimization and (*b*) WSS histograms of initial and optimized designs.

switched to fluid elements, while the fluid elements with a lower level of WSS are turned into solid elements. Following the proposed BESO procedure, the shear-induced mechanical erosion of polymers is also modeled. The examples demonstrate the applicability of proposed topology optimization method and shear-induced erosion model. It is important to mention that, within the context of scaffold micro-architectural design, there have been some reports available in which topology optimization technique was employed for the design of scaffold solid (polymer) phase. In this regard, Hollister and the coworkers [52] were among the first to introduce the homogenization approach to characterizing the trabecular bone micro-architectures. Further developed by Lin et al. [24], an inverse homogenization method was also implemented to seek optimal scaffold microstructures with desired (host-bone like) effective stiffness and porosity [28,53]. Following these successful attempts, increasing interest has been consistently placed to the design of solid phase in scaffold micro-architectures [53,54]. Having understood the necessity for generating a physiological uniform level of WSS distribution in the biofluidic phase for promoting cellular attachment and mechanobiological response, this paper presents a novel approach to the scaffold design for tissue engineering with a new criterion of biofluidic WSS.

Since the optimization problem presented herein aims to obtain a uniformly-distributed WSS on scaffold wall surfaces, while WSS represents a local quantity whose derivation of stress sensitivity is by no means easy (if not impossible), it is thus rather challenging to solve the optimization problem by using gradient-based algorithms. For this reason, various nongradient topology optimization approaches have been established to deal with stress

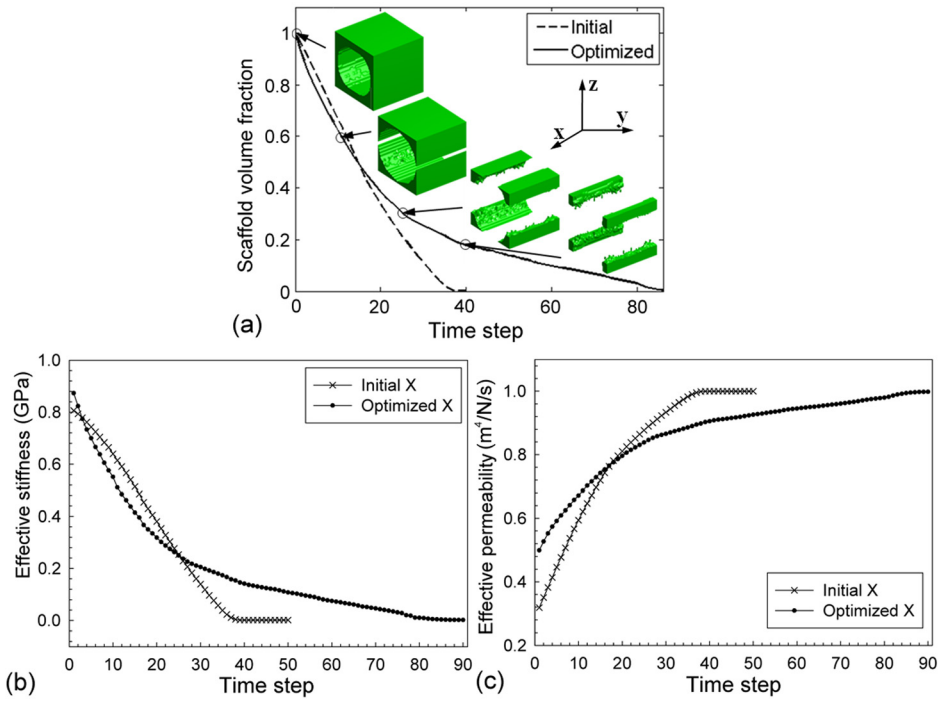

Fig. 7 Shear-induced erosion of optimized design under mono-directional flow. (*a*) Evolutions of scaffold volume loss in the initial and optimized designs and corresponding RVE structures. (*b*)–(*c*) Effective stiffness and permeability in the *x* direction of both initial and optimized scaffold designs. Since the lateral surfaces of optimized structure are weakened under mono-directional shear flow, only the component in the *x* direction is presented.

problems [48,55,56]. In this study, the bi-directional evolutionary structural optimization (BESO) is adopted.

In the first benchmark example, an obvious convergence history can be observed for the WSS objective function with a large volume variation, demonstrating the effectiveness of the proposed BESO approach. However, the objective function exhibits a certain fluctuation during the first 120 iterations as shown in Fig. 2(*c*), mainly caused by the continuous elemental manipulations between fluidic and solid elements subject to the prescribed volume constraint, which may deteriorate the smoothness of solid-fluid interface; thus influencing the interfacial flow characteristics. Meanwhile, introducing the volume variation ratio υ into Eq. (5) to reduce the volume change in each iteration results in a convergence trend in the BESO procedure, as seen in Fig. 2(*c*). It is also noteworthy that the resultant WSS distribution seems not completely uniform. This is because the optimized structure in this benchmark problem exhibits a certain curvature, where the flow flux is not perfectly uniform inside the fluid structure [48]. Nonetheless, the topological change taken place in this example is rather noteworthy, emerging an initial structure of 12 square bars into a single 90° turn tube. Although this example is not a direct scaffold-related application, it benchmarked the effectiveness of the proposed BESO-based optimization algorithm for the proposed WSS uniformity criterion.

In the second example for the tri-directional flow, a Schwarz-P structure is finally obtained. It is important to note that such an optimum seems to well correlate with those obtained from minimal energy dissipation [50], and extremal stiffness and permeability [30] in literature, which has been found particularly promising in the previous studies of scaffold design [51]. The Schwarz-P structure obtained in this example also provides some further implications in the design of scaffold micro-architecture for the proposed WSS criterion. It should be pointed out that although the flow condition is tri-directional and orthogonal, the erosive process in Fig. 3(*b*) undergoes somewhat nonorthogonal evolutions, showing the fact that the final design after the optimization is not perfectly orthogonal due to numerical errors.

It must be noted that due to different chemical properties, more *in vitro* experiments are needed to measure the WSS threshold for shear-induced erosion of different scaffold materials and different bio-fluids. In this respect, the WSS threshold $[\tau_{ero}]$ for shear-induced polymer erosion is selected empirically in this paper, which results in dimensionless data plotted in the *x*-axis (time step rather than specific time (e.g., day)) in the erosion figures. However, no matter what the specific threshold is adopted, the comparison of qualitative assessment of shear-induced erosion for the comparison of initial and optimal scaffold micro-architectures is valid. Under the same shear flow condition, optimal structures consistently exhibit a better stability and a longer lifetime in the erosion processes modeled.

In addition to the volume loss of scaffold under the shear-induced erosion shown in Figs. 3(*b*) and 7(*a*), the homogenization procedure provides us with a 'real-time' insight into the changes of macroscopic effective properties of scaffolds. As erosion progresses, more and more scaffold elements are eroded under shear flow, resulting in significant drop in effective stiffness and increase in effective permeability. It is found that the effective stiffness of the optimized scaffolds is higher than those of the initial designs in the examples. This would be rather beneficial to maintain long-lasting mechanical properties (when required) for scaffolds under shear flow. As a result, the operational lifetime of optimized scaffold is expected more persistent (approximately twice higher in the given examples) and provide a longer mechanical support to the desired tissue regeneration [53,57].

In this study, a simplified in-scaffold flow induced by a pair of velocity and pressure boundary conditions is considered. Although this approach has been successfully implemented in exploring the in-scaffold flow characteristics [37], more realistic mechanical boundary conditions, such as the contact interfaces between scaffold and surrounding tissue [58], the inlet and outlet

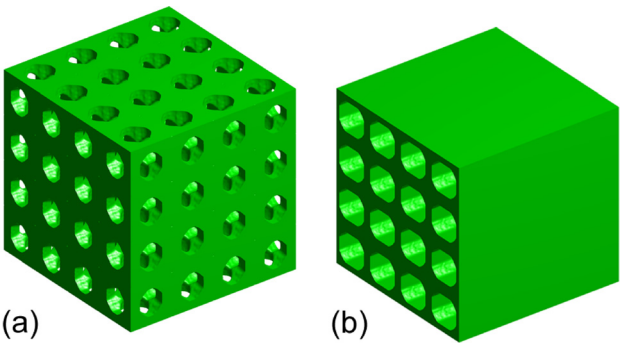

Fig. 8 Two representative optimal scaffold macro-structures ($4 \times 4 \times 4$ RVEs) designed by the WSS uniformity criterion. (*a*) Design under tri-directional flow as obtained from Fig. 3(*a*); (*b*) under mono-directional flow as obtained from Fig. 6(*a*).

locations of interstitial fluid and vascularization obtained from micro-CT or MRI imaging techniques can be applied to current flow model to characterize the realistic in-scaffold flow. It should be pointed out here that, no matter what values that one assigns to the velocity boundary condition, the optimal topology would remain similar since the optimal criterion given in Eq. (3) took the relative value of $\tau_w^e - \bar{\tau}_w$. In other words, the topology optimization algorithm relies on the difference of τ_w^e and $\bar{\tau}_w$. For the erosion model, the erosion process does not solely rely on the magnitude of inlet velocity, but on the relative relation between the WSS generated from the inlet velocity and threshold $[\tau_{ero}]$. Thus for a given $[\tau_{ero}]$, the comparison of erosion processes between initial and optimized scaffold microstructures is valid.

For the erosion model, the mesh density may affect the erosion process. This is because we adopted 'time step' rather than 'real time' as the unit of time frame in the erosion model. In each time step, only interfacial elements are allowed to erode; therefore it might take more time steps to erode the whole scaffold when a denser mesh is adopted for modeling scaffold solid. Nevertheless, the comparative relation between the erosion processes of initial and optimized cases still holds as long as the mesh sizes are the same.

Figure 8 shows the assembled optimized scaffold macrostructures ($4 \times 4 \times 4$ RVEs) obtained from the two representative examples, i.e., under tri- and mono-directional flows. It has been illustrated clearly that the optimal scaffold exhibits a considerably more uniform WSS distribution, which is considered rather beneficial to the cellular mechanobiological response to the in-scaffold bio-fluid. As the rapid development of solid free-form fabrication technique [19], the optimal designs have good topological features to be prototyped for *in vitro* and *in vivo* tests.

Note that flow-accelerated corrosion, erosion and degradation signify a special and important class of bioengineering problems, where erosion of polymeric scaffolds under a shear flow in bioreactor represents a typical application. In this respect, WSS plays a critical role in influencing erosion rate, which could determine the service life of some key components that are directly contacting with fluids. It is noted that although the effect of WSS on erosion has been well recognized in many experimental studies, the mechanism of real shear-erosion is rather complex, involving a range of chemical and physical complications, which have not been specifically addressed in this study. Other mechanical factors, such as pressure, flow velocity, solid-state stress and strain deformation etc., may also be the important parameters in regulating the performance of tissue scaffolds *in vivo* and *in vitro*. It must be also pointed out that slow erosion and long-lasting mechanical and structural features would depend on the applications and sometimes may not be required. The future work can be devoted to the studies on the tissue regeneration within optimized scaffold micro-architectures and/or explore other design criteria abovementioned, both numerically and experimentally.

Acknowledgment

The support from the Australian Research Council is gratefully acknowledged. Y.H. Chen is grateful for the Faculty Scholarship at the University of Sydney. M. Schellekens thanks Professor Ir. M.G.D. Geers at Eindhoven University of Technology, The Netherlands and Professor Y.W. Mai at the University of Sydney, Australia for facilitating his research internship at the University of Sydney.

References

[1] Langer, R., and Vacanti, J. P., 1993, "Tissue Engineering," Science, **260**(5110), pp. 920–926.
[2] Kwon, R. Y., and Jacobs, C. R., 2007, "Time-Dependent Deformations in Bone Cells Exposed to Fluid Flow in Vitro: Investigating the Role of Cellular Deformation in Fluid Flow-Induced Signaling," J. Biomech., **40**(14), pp. 3162–3168.
[3] Davies, P. F., 1995, "Flow-Mediated Endothelial Mechanotransduction," Physiol. Rev., **75**(3), pp. 519–560.
[4] Chen, H. B., Sundararaj, U., and Nandakumar, K., 2004, "Modeling of Polymer Melting, Drop Deformation, and Breakup Under Shear Flow," Polym. Eng. Sci., **44**(7), pp. 1258–1266.
[5] Lin, B., Sundararaj, U., Mighri, F., and Huneault, M. A., 2003, "Erosion and Breakup of Polymer Drops Under Simple Shear in High Viscosity Ratio Systems," Polym. Eng. Sci., **43**(4), pp. 891–904.
[6] Chen, Y. H., Zhou, S. W., and Li, Q., 2011, "Microstructure Design of Biodegradable Scaffold and its Effect on Tissue Regeneration," Biomaterials, **32**(22), pp. 5003–5014.
[7] Jacobs, C. R. Temiyasathit, S. and Castillo, A. B., 2010, "Osteocyte Mechanobiology and Pericellular Mechanics," Annu. Rev. Biomed. Eng., pp. 369–400.
[8] Meinel, L., Karageorgiou, V., Fajardo, R., Snyder, B., Shinde-Patil, V., Zichner, L., Kaplan, D., Langer, R., and Vunjak-Novakovic, G., 2004, "Bone Tissue Engineering Using Human Mesenchymal Stem Cells: Effects of Scaffold Material and Medium Flow," Ann. Biomed. Eng., **32**(1), pp. 112–122.
[9] Sakai, K., Mohtai, M., and Iwamoto, Y., 1998, "Fluid Shear Stress Increases Transforming Growth Factor Beta 1 Expression in Human Osteoblast-Like Cells: Modulation by Cation Channel Blockades," Calcif. Tissue Int., **63**(6), pp. 515–520.
[10] Gao, H., Ayyaswamy, P. S., and Ducheyne, P., 1997, "Dynamics of a mMicrocarrier Particle in the Simulated Microgravity Environment of a Rotating-Wall Vessel," Microgravity Sci. Technol., **10**(3), pp. 154–165.
[11] Adachi, T., Kameo, Y., and Hojo, M., 2010, "Trabecular Bone Remodelling Simulation Considering Osteocytic Response to Fluid-Induced Shear Stress," Philos. Trans. R. Soc. London, Ser. A **368**(1920), pp. 2669–2682.
[12] Provin, C., Takano, K., Sakai, Y., Fujii, T., and Shirakashi, R., 2008, "A Method for the Design of 3D Scaffolds for High-Density Cell Attachment and Determination of Optimum Perfusion Culture Conditions," J. Biomech., **41**(7), pp. 1436–1449.
[13] Vanapalli, S. A., Ceccio, S. L., and Solomon, M. J., 2006, "Universal Scaling for Polymer Chain Scission in Turbulence," Proc. Natl. Acad. Sci. U. S. A., **103**(45), pp. 16660–16665.
[14] Horn, A. F., 1984, "Midpoint Scission of Macromolecules in Dilute-Solution in Turbulent-flow," Nature, **312**(5990), pp. 140–141.
[15] Caruso, M. M. Davis, D. A. Shen, Q. Odom, S. A. Sottos, N. R. White, S. R. and Moore, J. S., 2009, "Mechanically-Induced Chemical Changes in Polymeric Materials," Chem. Rev., **109**(11), pp. 5755–5798.
[16] Osborne, J. M. O'Dea, R. D. Whiteley, J. P. Byrne, H. M. and Waters, S. L., 2010, "The Influence of Bioreactor Geometry and the Mechanical Environment on Engineered Tissues," ASME J. Biomech. Eng., **132**(5), 12.
[17] Kao, S. V. and Mason, S. G., 1975, "Dispersion of Particles by Shear," Nature, **253**(5493), pp. 619–621.
[18] Bawolin, N. K. Li, M. G. Chen, X. B. and Zhang, W. J., 2010, "Modeling Material-Degradation-Induced Elastic Property of Tissue Engineering Scaffolds," ASME J. Biomech. Eng., **132**(11), 7.
[19] Hollister, S. J., 2005, "Porous Scaffold Design for Tissue Engineering," Nature Mater., **4**(7), pp. 518–524.
[20] Hollister, S. J., 2009, "Scaffold Design and Manufacturing: from Concept to Clinic," Adv. Mater., **21**(32-33), pp. 3330–3342.
[21] Sun, W., Darling, A., Starly, B., and Nam, J., 2004, "Computer-Aided Tissue Engineering: Overview, Scope and Challenges," Biotechnol. Appl. Biochem., **39**, pp. 29–47.
[22] Khalil, S., and Sun, W., 2009, "Bioprinting Endothelial Cells With Alginate for 3D Tissue Constructs," ASME J. Biomech. Eng., **131**(11), 8.
[23] Challis, V. J., Roberts, A. P., Grotowski, J. F., Zhang, L. C., and Sercombe, T. B., 2010, "Prototypes for Bone Implant Scaffolds Designed via Topology Optimization and Manufactured by Solid Freeform Fabrication," Adv. Eng. Mater., **12**(11), pp. 1106–1110.
[24] Lin, C. Y. Kikuchi, N. and Hollister, S. J., 2004, "A Novel Method for Biomaterial Scaffold Internal Architecture Design to Match Bone Elastic Properties with Desired Porosity," J. Biomech., **37**(5), pp. 623–636.
[25] Zhou, S. W. and Li, Q., 2007, "The Relation of Constant Mean Curvature Surfaces to Multiphase Composites with Extremal Thermal Conductivity," J. Phys. D:Appl. Phys., **40**, pp. 6083–6093.
[26] Torquato, S. Hyun, S. and Donev, A., 2002, "Multifunctional Composites: Optimizing Microstructures for Simultaneous Transport of Heat and Electricity," Phys. Rev. Lett., **89**(26).
[27] Torquato, S. Hyun, S. and Donev, A., 2003, "Optimal Design of Manufacturable Three-Dimensional Composites with Multifunctional Characteristics," J. Appl. Phys., **94**(9), pp. 5748–5755.
[28] Chen, Y. H. Zhou, S. W. and Li, Q., 2009, "Computational Design for Multifunctional Microstructural Composites," Int. J. Mod. Phys. B, **23**(6–7), pp. 1345–1351.
[29] Chen, Y. H. Zhou, S. W. and Li, Q., 2010, "Multiobjective Topology Optimization for Finite Periodic Structures," Comput. Struct., **88**(11–12), pp. 806–811.
[30] Guest, J. K. and Prevost, J. H., 2006b, "Optimizing Multifunctional Materials: Design of Microstructures for Maximized Stiffness and Fluid Permeability," Int. J. Solids Struct., **43**(22–23), pp. 7028–7047.
[31] Kang, H. Lin, C. Y. and Hollister, S. J., 2010, "Topology Optimization of Three Dimensional Tissue Engineering Scaffold Architectures for Prescribed Bulk Modulus and Diffusivity," Struct. Multidiscip. Optim., **42**(4), pp. 633–644.
[32] Huang, X. and Xie, Y. M., 2009, "Bi-Directional Evolutionary Topology Optimization of Continuum Structures with One or Multiple Materials," Comput. Mech., **43**(3), pp. 393–401.
[33] Huang, X. D. and Xie, Y. M., 2010, *Evolutionary Topology Optimization of Continuum Structures: Methods and Applications*, Wiley, NY.
[34] Jacobs, C. R., Yellowley, C. E., Davis, B. R., Zhou, Z., Cimbala, J. M., and Donahue, H. J., 1998, "Differential Effect of Steady Versus Oscillating Flow on Bone Cells," J. Biomech., **31**(11), pp. 969–976.
[35] Khaled, A. R. A., and Vafai, K., 2003, "The Role of Porous Media in Modeling Flow and Heat Transfer in Biological Tissues," Int. J. Heat Mass Transfer **46**(26), pp. 4989–5003.
[36] Yeatts, A. B. and Fisher, J. P., 2011, "Bone Tissue Engineering Bioreactors: Dynamic Culture and the Influence of Shear Stress," Bone, **48**(2), pp. 171–181.
[37] Maes, F. Ransbeeck, P. Van Oosterwyck, H. and Verdonck, P., 2009, "Modeling Fluid Flow Through Irregular Scaffolds for Perfusion Bioreactors," Biotechnol. Bioeng., **103**, pp. 621–630.
[38] Querin, O. M. Steven, G. P. and Xie, Y. M., 1998, "Evolutionary Structural Optimisation (ESO) Using a Bidirectional Algorithm," Eng. Comput., **15**(8), pp. 1031–1048.
[39] Li, Q. Steven, G. P. and Xie, Y. M., 2001, "A Simple Checkerboard Suppression Algorithm for Evolutionary Structural Optimization," Struct. Multidiscip. Optim., **22**(3), pp. 230–239.
[40] Chen, Y. H. Zhou, S. W. and Li, Q., 2011, "Mathematical Modeling of Degradation for Bulk-Erosive Polymers: Applications in Tissue Engineering Scaffolds and Drug Delivery Systems," Acta Biomater., **7**(3), pp. 1140–1149.
[41] Culter, J. D., Zakin, J. L., and Patterson, G. K., 1975, "Mechanical Degradation of Dilute-Solutions of High Polymers in Capillary Tube Flow," J. Appl. Polym. Sci., **19**(12), pp. 3235–3240.
[42] Hassani, B., and Hinton, E., 1998, "A Review of Homogenization and Topology Optimization II - Analytical and Numerical Solution of Homogenization Equations," Comput. Struct., **69**(6), pp. 719–738.
[43] Zhou, S. and Li, Q., 2008, "Computational Design of Multi-Phase Microstructural Materials for Extremal Conductivity," Comput. Mater. Sci., **43**(3), pp. 549–564.
[44] Porter, B. Zauel, R. Stockman, H. Guldberg, R. and Fyhrie, D., 2005, "3-D Computational Modeling of Media Flow Through Scaffolds in a Perfusion Bioreactor," J. Biomech., **38**(3), pp. 543–549.
[45] Boschetti, F. Raimondi, M. T. Migliavacca, F. and Dubini, G., 2006, "Prediction of the Micro-Fluid Dynamic Environment Imposed to Three-Dimensional Engineered Cell Systems in Bioreactors," J. Biomech., **39**(3), pp. 418–425.
[46] Cioffi, M. Boschetti, F. Raimondi, M. T. and Dubini, G., 2006, "Modeling eEvaluation of the fFluid-dDynamic mMicroenvironment in Tissue-Engineered Constructs: A Micro-CT Based Model," Biotechnol. Bioeng., **93**(3), pp. 500–510.
[47] Milan, J. L. Planell, J. A. and Lacroix, D., 2009, "Computational Modelling of the Mechanical Environment of Osteogenesis within a Polylactic Acid-Calcium Phosphate Glass Scaffold," Biomaterials, **30**(25), pp. 4219–4226.
[48] Steven, G. P. Li, Q. and Xie, Y. M., 2000, "Evolutionary tTopology and sShape dDesign for gGeneral pPhysical fField pProblems," Comput. Mech., **26**(2), pp. 129–139.
[49] Borrvall, T. and Petersson, J., 2003, "Topology Optimization of Fluids in Stokes Flow," Int. J. Numer. Methods Fluids, **41**(1), pp. 77–107.
[50] Zhou, S. W. and Li, Q., 2008, "A Variational Level Set Method for the Topology Optimization of Steady-State Navier-Stokes Flow," J. Comput. Phys., **227**(24), pp. 10178–10195.
[51] Rajagopalan, S. and Robb, R. A., 2006, "Schwarz Meets Schwann: Design and Fabrication of Biomorphic and Durataxic Tissue Engineering Scaffolds," Med. Image Anal., **10**, pp. 693–712.
[52] Hollister, S. J. Fyhrie, D. P. Jepsen, K. J. and Goldstein, S. A., 1991, "Application of Homogenization Theory to the Study of Trabecular Bone Mechanics," J. Biomech., **24**(9), pp. 825–839.
[53] Sturm, S. Zhou, S. W. Mai, Y. W. and Li, Q., 2010, "On Stiffness of Scaffolds for Bone Tissue Engineering - A Numerical Study," J. Biomech., **43**, pp. 1738–1744.
[54] Sanz-Herrera, J. A. Garcia-Aznar, J. M. and Doblare, M., 2009, "On Scaffold Designing For Bone Regeneration: A Computational Multiscale Approach," Acta Biomater., **5**(1), pp. 219–229.

[55] Victoria, M. Querin, O. M. and Marti, P., 2010, "Topology Design for Multiple Loading Conditions of Continuum Structures Using Isolines and Isosurfaces," Finite Elem. Anal. Des., **46**(3), pp. 229–237.
[56] Chen, Y. H. Zhou, S. W. Cadman, J. and Li, Q., 2010, "Design of Cellular Porous Biomaterials for Wall Shear Stress Criterion," Biotechnol. Bioeng., **107**(4), pp. 737–746.
[57] Adachi, T. Osako, Y. Tanaka, M. Hojo, M. and Hollister, S. J., 2006, "Framework for Optimal Design of Porous Scaffold Microstructure by Computational Simulation of Bone Regeneration," Biomaterials, **27**(21), pp. 3964–3972.
[58] Sutradhar, A. Paulino, G. H. Miller, M. J. and Nguyen, T. H., 2010, "Topological Optimization for Designing Patient-Specific Large Craniofacial Segmental Bone Replacements," Proc. Natl. Acad. Sci. U.S.A., **107**(30), pp. 13222–13227.